

Carbosilicene and germasilicene: Two 2D materials with excellent structural, electronic and optical properties

Saeid Amjadian¹,¹ Mahdi Esmailzadeh²,² and Nezhat Pournaghavi²

¹*Department of Physics, Iran University of Science and Technology, Narmak, Tehran 16844, Iran*

²*Department of Applied Physics, School of Engineering Sciences,*

KTH Royal Institute of Technology, AlbaNova University Center, SE-10691 Stockholm, Sweden

(Dated: January 24, 2022)

Using first principle calculations, we study the structural, optical and electronic properties of two-dimensional silicene-like structures of CSi₇ (carbosilicene) and GeSi₇ (germasilicene) monolayers. We show that both CSi₇ and GeSi₇ monolayers have different buckling that promises a new way to control the buckling in silicene-like structures. Carbon impurity decreases the silicene buckling, whereas germanium impurity increases it. The CSi₇ has semiconducting properties with 0.25 eV indirect band gap, but GeSi₇ is a semimetal. Also, under uniaxial tensile strain, the semiconducting properties of CSi₇ convert to metallic properties which shows that CSi₇ can be used in straintronic devices such as strain sensor and strain switch. There is no important response for GeSi₇ under strain. The GeSi₇ has higher dielectric constant relative to CSi₇, silicene and graphene and it can be used as a 2D-material in high performance capacitors. Calculation of cohesive and formation energies show that CSi₇ is more stable than GeSi₇. Furthermore, we investigate the optical properties of these new materials and we show that CSi₇ and GeSi₇ can significantly increase the light absorption of silicene. The obtained results can pave a new route for tuning the electronic and optical properties of silicene like structures for different applications in nanoelectronic devices.

I. INTRODUCTION

Two dimensional (2D) materials like graphene, silicene and germanene are semimetals with zero-gap [1, 2], and their charge carriers are massless fermions[3]. Graphene have been studied vastly because of its superior advantages such as mechanical, optical and electronic properties [4–18]. Different doping are performed in graphene for the new applications such as sulfur-doping for micro-supercapacitors[19], nitrogen-doped graphene quantum dots for photovoltaic[20], silicon nanoparticles embedded in n-doped few-layered graphene for lithium ion batteries[21] and implanting germanium into graphene for single-atom catalysis applications[22]. Theoretical and experimental investigations of graphene-like structures such as silicene and germanene have been vastly carried out [23–28]. Silicene and germanene have been grown on Au(111)[29], Ag(111)[30] and Ir(111)[31] that can encourage researchers to do more study about them. Due to the buckled structure of silicene, it has different physical properties compared to graphene, such as higher surface reactivity[30], and a tunable band gap by using an external electric field which is highly favorable in nanoelectronic devices[3, 32]. However, the formation of imperfections on the synthesis of silicene is usually inevitable which influences the magnetic and electronic properties of the material[33]. There are some studies about doped atoms such as lithium, aluminum and phosphorus in silicene to achieve wide variety of electronic and optical properties[34, 35]. Recently simulation and fabrication of 2D silicon-carbon compounds known as siligraphene (Si_mC_n) have received more attentions due to their extraordinary electronic and optical properties. For example, SiC₂ siligraphene which has been experimentally synthesized[36], is a promising anchoring material for lithium-sulfur batteries[37], a promising metal-free catalyst for oxygen reduction reaction[37], and a novel donor material in excitonic solar cells[38]. Also, graphitic siligraphene g-SiC₃ in the presence of strain can

be classified in different electrical phases such as a semimetal or a semiconductor. g-SiC₃ has a semimetallic behavior under compression strain up to 8%, but it becomes a semiconductor with direct band gap (1.62 eV) for 9% of compression strain and becomes a semiconductor with indirect band gap (1.43 eV) for 10% of compression strain [37]. Moreover, g-SiC₅ has semimetallic properties and it can be used as a gas sensor for air pollutant[39]. Furthermore, SiC₇ siligraphene has a good photovoltaic applications [40] and can be used as a high capacity hydrogen storage material[41]. It shows superior structural, dynamical and thermal stability comparing to other types of siligraphene and it is a novel donor material with extraordinary sunlight absorption[42]. The structural and electronic properties of silicene-like SiX and XSi₃ (X = B, C, N, Al, P) honeycomb lattices have been investigated[43]. Also, the planarity and non-planarity properties for g-SiC_n and g-Si_nC (n = 3, 5, and 7) structures have been studied[44].

The excellent properties of siligraphene[42] motivated us to study CSi₇ and GeSi₇, in order to find a new approach of silicene buckling and band gap control and to obtain new electronic and optical properties. Here we call CSi₇ carbosilicene and GeSi₇ germasilicene. We choose carbon and germanium atoms respectively for CSi₇ and GeSi₇ because these atoms, same as silicon atom, have four valence electrons in their highest energy orbitals. Using density functional theory, we show that both structures are stable but CSi₇ is more stable than GeSi₇. The carbon atom in CSi₇ decreases the buckling, while germanium atom in GeSi₇ increases the buckling. It is shown that CSi₇ is a semiconductor with 0.24 eV indirect band gap[45] but GeSi₇, similar to silicene, is a semimetal. Also, we investigate the effects of strain and we show that for CSi₇, the compressive strain can increase the band gap and the tensile strain can decrease. At sufficient tensile strain (>3.7%), the band gap of CSi₇ becomes zero and thus the semiconducting properties of this material change to metallic properties. As a result, the band gap of CSi₇ can be tuned by strain and this

material can be used in straintronic devices such as strain sensors and strain switches. For GeSi₇, strain does not have any significant effect on it. In contrast, GeSi₇ has high dielectric constant and can be used as a 2D material with high dielectric constant in advanced capacitors. Finally, we investigate the optical properties of these materials and we find that the light absorption of both CSi₇ and GeSi₇ are significantly greater than the light absorption of silicene. Because of high absorption of CSi₇ and GeSi₇, these materials can be considered as a good candidate for solar cell applications. It is worth to mention that gerasilicene, GeSi₇, is a new 2D material proposed and studied in this paper, while carbosilicene, CSi₇, has been proposed previously as a member of siligraphene but only its band structure has been studied[44–46]. The rest of the paper is organized as follows. In Sec. II, method of calculations is introduced and the results and discussion are given in Sec. III. Section IV contains a summary and conclusion.

II. METHOD OF CALCULATIONS

Density functional theory (DFT) calculations are performed using the projector-augmented wave pseudopotentials [47] as implemented in the Quantum-ESPRESSO code[48]. To describe the exchange-correlation functional, the generalized gradient approximation (GGA) of Perdew-Bruke-Ernzerhof (PBE) is used[49]. After optimization, the optimum value for the cutoff energy is obtained equal to 80 Ry. Also, Brillouin-zone integrations are performed using Monkhorst-Pack[50] and optimum reciprocal meshes of 12×12×1 are considered for calculations. At first, unit cells and atomic positions of both CSi₇ and GeSi₇ are optimized and then their electronic properties are determined by calculating the density of states and band structure. Moreover, their optical properties are determined by calculating the absorption and the imaginary and real parts of dielectric constant.

III. RESULTS AND DISCUSSION

A. Structural properties

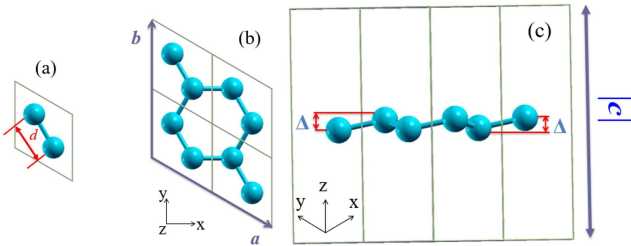


FIG. 1. (a) Top view of silicene and (b) Si₈ unit cells. (c) Side view of Si₈ unit cell.

By increasing silicene unit cell [see Fig. 1 (a)] in x and y direction twice, Si₈ has been constructed [see Fig. 1(b)] in

hexagonal lattice (i.e., $\alpha = \beta = 90^\circ, \gamma = 120^\circ$). In physical view, both silicene and Si₈ have the same physical properties because by increasing both unit cells, silicene monolayer has been achieved. In this work, Si₈ unit cell considered because CSi₇ and GeSi₇ can be constructed by replacing a silicone atom with a carbon or a germanium atom. After relaxation, the bond length of Si₈ was $d = 2.4 \text{ \AA}$ [see Fig. 1 (a)] and lattice parameters were $|a| = |b| = 7.56 \text{ \AA}$ and $|c| = 14.4 \text{ \AA}$ [see Figs. 1(b) and 1(c)] and buckling parameter $\Delta = 0.44 \text{ \AA}$ [see Fig. 11 (c)] which has a good agreement with previous works[51–53]. Here c is the distance to make sure that there is no interaction between adjacent layers. For carbosilicene, CSi₇, unit cell construction, a silicon atom can be replaced with a carbon atom as shown in Fig. 2. Because of structural symmetry of CSi₇ monolayer (see Fig. 6), the position of impurity atom is not important, and our calculations also show the same ground state energy for all the eight possible impurity positions. After relaxation, optimum lattice parameters are obtained as $|a| = |b| = 7.49 \text{ \AA}$ and $|c| = 12.86 \text{ \AA}$ for CSi₇ unit cell. Fig. 2 shows this structure before and after relaxation. For a more detailed explanation, we labeled atoms in this figure. It is observed that Si-C bond length (i.e., $d_{2-4} = 1.896 \text{ \AA}$) is shorter than Si-Si band length (i.e., $d_{1-2} = 2.317, d_{1-3} = 2.217 \text{ \AA}$) because of sp² hybridization. Also, unlike graphene, the hexagonal ring is not a regular hexagon due to the electronegativity difference between C and Si atoms[42].

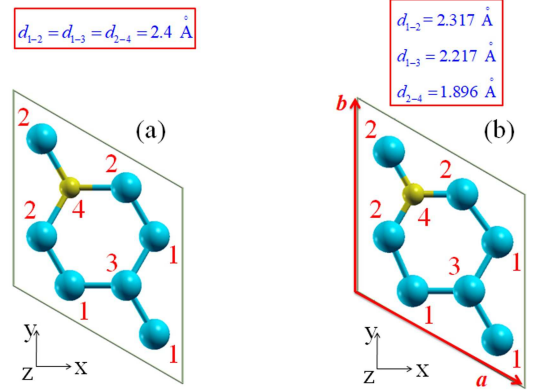


FIG. 2. Top view of CSi₇ unit cell (a) before and (b) after relaxation. Carbon atom is shown by yellow sphere and silicon atoms by blue spheres.

Fig. 3 shows the side view of CSi₇ unit cell. After relaxation, the buckling parameter between atoms 1 and 3 (Δ_{1-3}) is 0.1 \AA whereas this parameter for atoms 2 and 4 (Δ_{2-4}) is 0.39 \AA . So, CSi₇ has a structure with two different buckling parameters and one can use the carbon atoms to decrease buckling parameter of silicene. Silicene has one buckling and two sublattices[54], while carbosilicene has two bucklings and thus three sublattices including one for carbon atoms and two others for silicon atoms.

If we replace a silicon atom with a germanium atom as shown in Fig. 4, we could obtain gerasilicene, GeSi₇, structure. As we can see in this figure, the optimized parameters

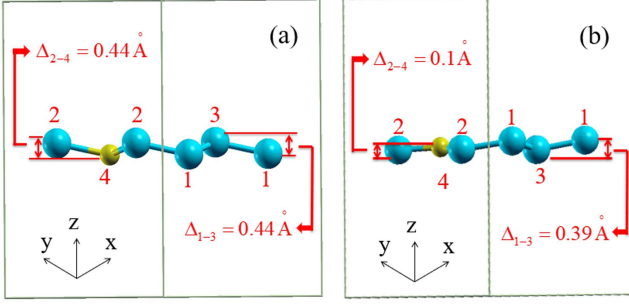


FIG. 3. Side view of CSi₇ unit cell (a) before and (b) after relaxation.

are $|a|=|b|=7.8\text{Å}$, $|c|=11.98\text{Å}$ and the Si-Ge bond length and lattice constants are greater than those of Si-Si. Also, by comparing bond lengths and lattice parameters of GeSi₇ and CSi₇ structures, it is seen that the bond lengths and lattice parameters of GeSi₇ are significantly greater than those of CSi₇ which is due to the larger atomic number and thus atomic radius of germanium relative to the carbon[55].

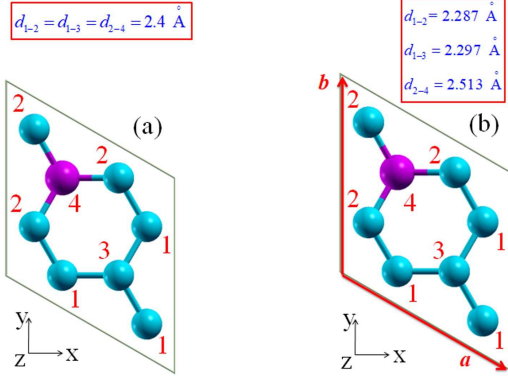


FIG. 4. Top view of GeSi₇ unit cell (a) before and (b) after relaxation. Here germanium atom is shown by purple color.

The buckling parameters of germa-silicene structure are depicted in Fig. 5. After relaxation, we find that the value of these parameters are $\Delta_{2-4} = 0.53\text{Å}$ and $\Delta_{1-3} = 0.43\text{Å}$. Therefore, GeSi₇ like CSi₇ has a structure with two different buckling and the germanium impurity atom increases the buckling of silicene. Bond length values and other structural parameters after relaxation are shown in Table 1.

We now introduce a new parameter for buckling as

$$\Delta_d = |\Delta_{2-4} - \Delta_{1-3}| \quad (1)$$

which shows the difference between two buckling parameters. Value of Δ_d for CSi₇ (i.e., 0.29Å) is greater than that for GeSi₇ (i.e., 0.062Å) which means the carbon impurity atom has a greater impact than germanium on silicene buckling. This effect could be explained based on electronegativity difference[56]. The electronegativity by Pauling scale is 2.55 [57, 58], 1.9 [59] and 2.01 [60] for carbon, silicon, and germanium respectively. Therefore, electronegativity difference is 0.65 for CSi₇ and 0.11 for GeSi₇ which show that CSi₇ has a

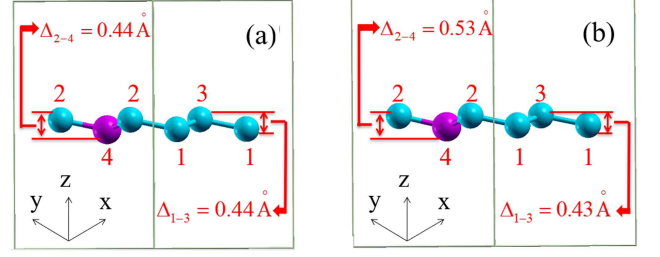


FIG. 5. Side view of GeSi₇ unit cell (a) before and (b) after relaxation

greater electronegativity difference which leads to the in-plane hybridized bondings and reduces the buckling in comparison to the other cases.

Fig. 6 shows the charge density of a monolayer of CSi₇ and GeSi₇. The charge density of a monolayer of Si is also shown in this figure for comparison [see Fig. 6(a)]. The high charge density around the carbon and germanium impurity atoms [see Figs. 6(b) and 6(c)] shows charge transfer from silicon atoms to impurity atoms. Also, the electron aggregation around impurity atoms indicates ionic-covalent bonds in CSi₇ and GeSi₇ structures because of electronegativity difference.

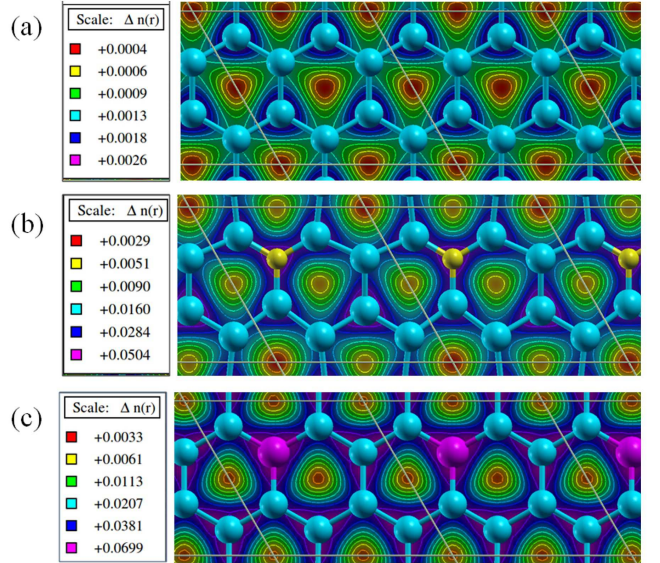


FIG. 6. Charge density of (a) silicene, (b) CSi₇ and (c) GeSi₇

Now, we calculate the cohesive and formation energies for these structures. The cohesive energy is -4.81eV/atom and -4.32eV/atom for CSi₇ and GeSi₇, respectively. The negative value of cohesive energy for CSi₇ and GeSi₇ means that these structures will not be decomposed into their atoms. The more negative cohesive energy, the more stable structure, so CSi₇ is more stable than GeSi₇. Also, the calculated cohesive energy for silicene is -4.89eV/atom which is in good agreement with previous studies [59, 60] and shows CSi₇ has a stable structure with cohesive energy very close to silicene. Our calculations show the formation energy for CSi₇ and GeSi₇ structures are

	$ a = b $	$ c $	d_{1-2}	d_{2-4}	d_{1-3}	Δ_{2-4}	Δ_{1-3}	Δ_d
Si ₈	7.65	14.4	2.4	2.4	2.4	0.44	0.44	0
CSi ₇	7.49	12.86	2.317	1.896	2.217	0.1	0.39	0.29
GeSi ₇	7.8	11.98	2.287	2.34	2.297	0.53	0.43	0.1

TABLE I. Optimum lattice parameters $|a|$, $|b|$ and $|c|$, bond lengths d_{1-2} , d_{2-4} and d_{1-3} and buckling parameters Δ_{2-4} , Δ_{1-3} and Δ_d . All values are in Angstrom.

+0.16 eV/atom and -0.005 eV/atom, respectively. So, the formation of CSi₇ (GeSi₇) from their constituents is endothermic (exothermic) because of the positive (negative) value of formation energy. On the other hand, positive formation energy for CSi₇ represents a high stability of this structure, while the negative or nearly zero value for GeSi₇ is attributed mostly to the high reactivity related to silicene[43].

B. Electronic properties

To investigate electronic properties of CSi₇ and GeSi₇, at first, we compare band structure of silicene, CSi₇ and GeSi₇ monolayers and we show the results in Fig. 7. As we can see in this figure, like graphene and silicene, GeSi₇ is semi-metal (or zero-gap semiconductor) with Dirac cone in point K. This is because the π and π^* bands cross linearly at the Fermi energy E_F . These band structures indicate that the charge carrier in silicene and GeSi₇ behave like massless Dirac fermions[53]. In contrast with GeSi₇, CSi₇ is a semiconductor with indirect band gap. The value of its indirect band gap is 0.24 eV in $K - \Gamma$ direction which significantly less than its direct band gap value (i.e., 0.5 eV in $K - K$ direction).

For a better comparison, an enlarged band structure of silicene, CSi₇ and GeSi₇ are shown in Fig. 8. It is seen that, in point K, silicene and GeSi₇ have similar band structures with zero band gap, whereas CSi₇ has a band gap. In Dirac cone of graphene and silicene, π and π^* bands are made from the same atoms[43] but these bonds in GeSi₇ are made from two different atoms. To determine the Fermi velocity, v_F , the graphs for silicene and GeSi₇ must be fitted linearly near the Fermi level by using equation $E_{k+K} = \gamma k$. Then the Fermi velocity is given by $v_F = \gamma/\hbar$. Our calculations show that v_F is 5×10^5 m/s for silicene (which shows a good agreement with previous works[43, 61]) and 4.8×10^5 m/s for GeSi₇. A comparison between Fermi velocity in silicene and GeSi₇ indicates that Ge atoms in GeSi₇ do not have a significant effect on Fermi velocity. The total density of states (DOS) is also shown in Fig. 8. It is observed that the total DOS has a good agreement with the band structure.

We now investigate the effect of strain on the band structure of CSi₇ and GeSi₇ and the results are shown in Fig. 9. As we can see in Figs. 9(a) and 9(b), compressive strain has important effects on band structure of CSi₇ but it has no significant effect on GeSi₇ [compare these figures with Figs. 7(b) and 7(c)]. In the presence of compressive strain for CSi₇, both direct and indirect band gaps increase, respectively from 0.5 eV and 0.24 eV to 0.52 eV and 0.44 eV. But for GeSi₇, the zero-band gap remains unchanged and compressive strain cannot open any band gap. Fig. 9(c) shows the direct and

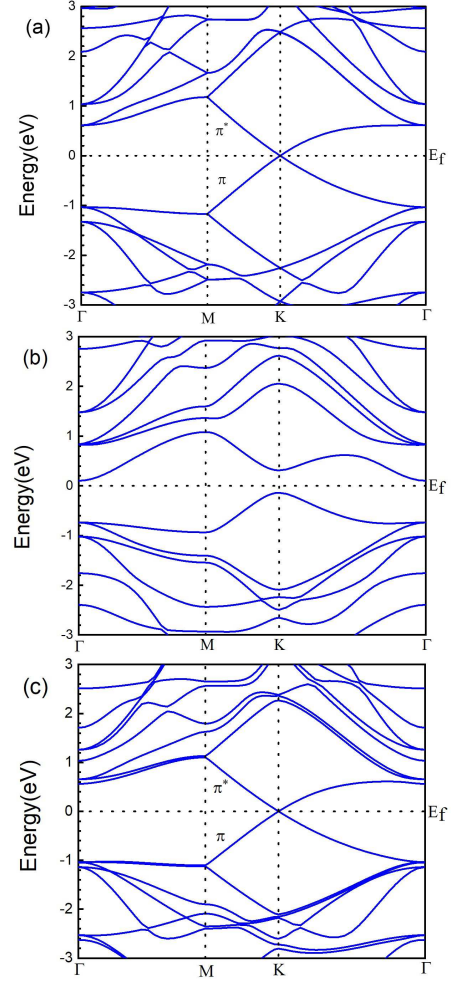


FIG. 7. Band structure of (a) silicene, (b) CSi₇ and (c) GeSi₇.

indirect band gap variations of CSi₇ versus the both compressive and tensile strains. It is observed that both direct and indirect band gaps increase with increasing the compressive strain, while they decrease with increasing the tensile strain. The variation of band gaps versus strain S is nearly linear and could be formulated by $E_g = -0.017S + 0.447$ for direct band gap and $E_g = -0.059S + 0.227$ for indirect one. Under strain and without strain, the direct band gap has significantly larger values relative to indirect band gap, thus it has no important effect on electronic transport properties in CSi₇. In contrast with GeSi₇, the strain is an important factor for tuning of band gap in CSi₇. For example, when the tensile strain increases above the band gap of CSi₇ disappears and this 2D material becomes a metal [see Fig. 9(c)]. This property of CSi₇ is

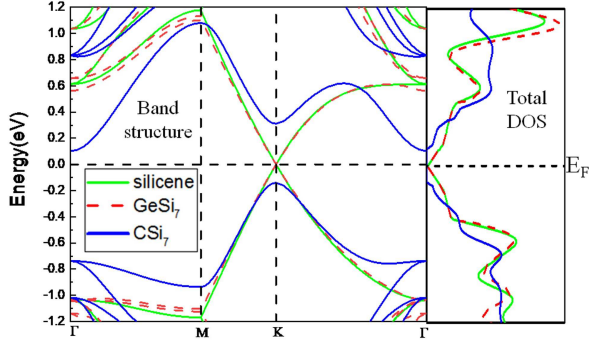


FIG. 8. Enlarged band structure and total DOS of silicene, CSi7 and GeSi7.

important in straintronic devices such as strain switches and strain sensors.

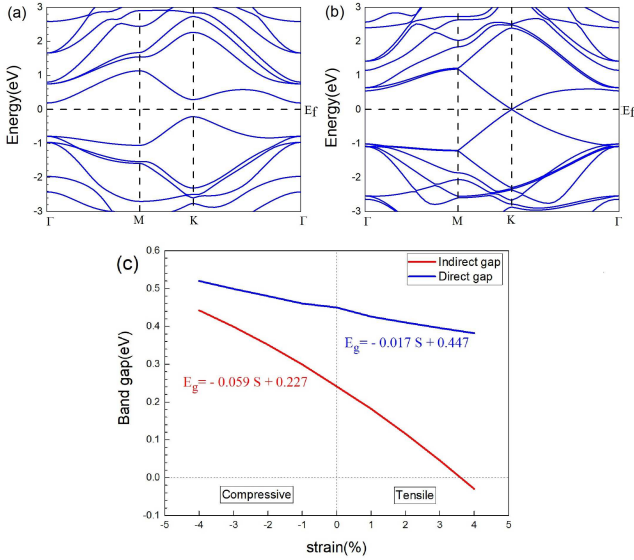


FIG. 9. Band structure of (a) CSi7 and (b) GeSi7 under compressive strain with value -3%. (c) Energy gap variation of CSi7 versus both compressive and tensile strains.

C. Optical properties

The complex dielectric function $\epsilon = \epsilon_r + \epsilon_i$ can be calculated for both polarizations of light: (i) parallel (x direction) and (ii) perpendicular (z direction), where ϵ_r is the real part and ϵ_i is the imaginary part of the dielectric function. This function is an important parameter for calculation of optical properties of matters. For instance, the real and imaginary parts of refractive index (i.e., $n = n_r + n_i$) can be written as[62]

$$n_r = \sqrt{\frac{(\epsilon_r^2 + \epsilon_i^2)^{1/2} + \epsilon_r}{2}} \quad (2)$$

and

$$n_i = \sqrt{\frac{(\epsilon_r^2 + \epsilon_i^2)^{1/2} - \epsilon_r}{2}} \quad (3)$$

respectively. The absorption coefficient α is given by[62]

$$\alpha = \frac{2\omega n_i}{C} \quad (4)$$

where C is the speed of light in vacuum. The real parts of dielectric function of CSi7, GeSi7 and silicene are depicted in Fig. 10 for x and z directions. This figure shows that ϵ_r in both directions are inhomogeneous because the graphs of ϵ_r are not similar for the two directions. The root of real part (where $\epsilon_r = 0$) represents the plasma energy (frequency) which for these materials it locates at 4.3 eV (1.04 PHz) for x-direction. It can be seen from Figs. 10(a) and 10(b) that the values of static dielectric constant (the value of dielectric function real part at zero frequency or zero energy) in the x-direction are 12.3 for silicene and CSi7 and 30 for GeSi7, and in the z-direction are 2.4, 2 and 2.9 for silicene, CSi7 and GeSi7 respectively. Thus, for both directions GeSi7 has the biggest static dielectric constant. Also, the static dielectric constant of GeSi7 is significantly greater than graphene (1.25 for z-direction and 7.6 for x-direction[63]). According to the energy density equation of capacitors (i.e., $u = \epsilon\epsilon_0 E^2/2$), by increasing dielectric constant ϵ , the energy density u increases. Here, E in the electric field inside the capacitor. So, materials with high dielectric constant have attracted a lot of attentions because of their potential applications in transistor gate, non-volatile ferroelectric memory and integral capacitors[64]. Among the 2D-materials, graphene has been used for electrochemical capacitors[65] and supercapacitors[66]. Since GeSi7 has a high dielectric constant, it can be used as a 2D-material with high performance dielectric in advanced capacitors.

Fig. 11 shows absorption coefficient α for CSi7 and GeSi7. Absorption coefficient for silicene is also shown in this figure for comparison. The absorption coefficient shown in this figure for silicene is in agreement with previous works[67, 68]. There are two peaks for CSi7: one locates in 1.18 eV (infrared region) and the other in 1.6 eV (visible region). The peak for silicene (at 1.83 eV) locates in visible region (1.8-3.1 eV). So, carbon atom increases and shifts the edge of absorption from the visible region to infrared region because it breaks the symmetry of silicene structure and it opens a narrow energy band gap in silicene band structure. For GeSi7 there is an absorption peak in visible region (at 2.16 eV). Also, the peak height of GeSi7 is larger than that of silicene and CSi7. The sun light spectrum includes different wavelengths and absorption of each part has a special application. For example, ultraviolet-visible region absorption spectrophotometry and its analysis are used in pharmaceutical analysis, clinical chemistry, environmental analysis and inorganic analysis[69]. Also near infrared ($\lambda = 800$ to 1100 nm or $E = 1.55$ eV to 1.13 eV) and infrared ($\lambda > 1100$ nm or $E < 1.13$ eV) regions are used for solar cells[70, 71], latent fingerprint development[72], brain stimulation and imaging[73], photothermal therapy[74], photocatalysis[75] and photobiomodulation[76].

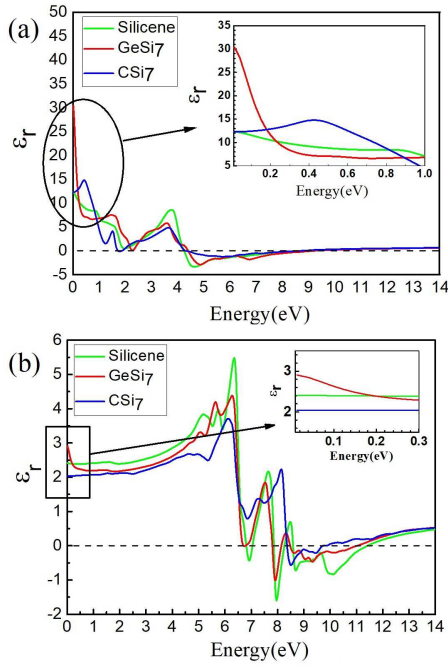


FIG. 10. Comparison of real part of dielectric function for CSi7 and GeSi7 (a) in x direction and (b) in z direction. The graphs of silicene are also shown in this figure for comparison.

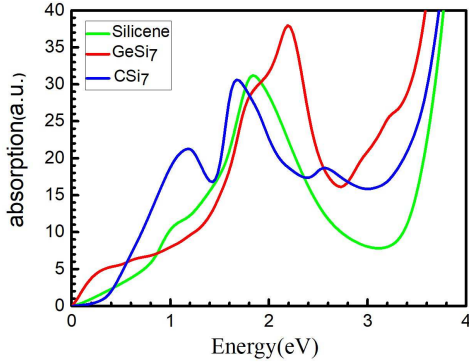


FIG. 11. Absorption coefficient for silicene, CSi7 and GeSi7.

On the other hand, sunlight radiation received by earth is comprising 5% ultraviolet, 45% infrared and 50% visible [77]. So, we investigate area under the absorption curve of CSi7 and GeSi7 in visible (from 1.8 to 3.1 eV), near infrared (from 1.13 to 1.55 eV) and infrared (<1.13 eV). Fig. 12 shows this area for silicene, CSi7 and GeSi7 in infrared, near infrared and visible spectrum regions. As we can see in this figure, the absorption of CSi7 for all three spectrum regions and total absorption are significantly greater than those of silicene. The absorption of GeSi7 is greater than that of silicene in infrared and visible regions and it is smaller in near infrared region, but the total absorption of GeSi7 is significantly greater than the total absorption of silicene. For comparison, we also calculate the absorption coefficient in infrared region for siligraphene SiC₇, a new material studied recently[42]. The absorption for

siligraphene in infrared region is equal to 2.7 which shows that CSi7 with absorption 8.78 and GeSi7 with absorption 6.31 have more than two times greater absorption relative to siligraphene in infrared region.

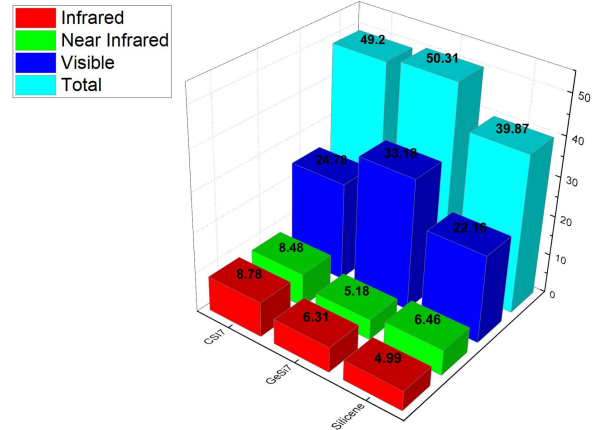


FIG. 12. Areas under the absorption curve for silicene, CSi7 and GeSi7 in infrared, near infrared and visible spectrum regions.

D. Summary and conclusion

We studied the structural, electronic and optical properties of CSi7 and GeSi7 structures using density functional theory within Quantum Espresso code. We showed that the carbon atom in CSi7 decreases the buckling, whereas germanium atom in GeSi7 increases the buckling which promises a new way to control the buckling in silicene-like structures. Both structures are stable but CSi7 is more stable than GeSi7. Band structure and DOS plots show CSi7 is a semiconductor with 0.24 eV indirect band gap but GeSi7, similar to silicene, is a semimetal. Strain does not have any significant effect on GeSi7, but for CSi7, the compressive strain can increase the band gap and tensile strain can decrease it. At sufficient tensile strain (> 3.7%), the band gap becomes zero or negative and thus the semiconducting properties of CSi7 change to metallic properties. As a result, the band gap of CSi7 could be changed and controlled by strain and this material can be used in straintronic devices such as strain sensor and strain switch. Furthermore, we investigated the optical properties of CSi7 and GeSi7 such as static dielectric constant and light absorption. The GeSi7 has high dielectric constant relative to CSi7, silicene and graphene and can be used as a 2D-material with high performance dielectric in advanced capacitors. The light absorption of CSi7 for near infrared, infrared and visible regions and its total absorption are significantly greater than those of silicene. The absorption of GeSi7 is greater than that of silicene in infrared and visible regions and it is smaller in near infrared region, but the total absorption of GeSi7 is significantly greater than the total absorption of silicene. Because of high absorption of CSi7 and GeSi7, these materials can be considered as proper candidates to solar cell applications.

-
- [1] S. Wang, *Physical Chemistry Chemical Physics* **13**, 11929 (2011).
- [2] S. Cahangirov, M. Topsakal, and E. A. Ciraci, *Physical Review Letters* **102** (2009).
- [3] Z. Ni, Q. Liu, K. Tang, J. Zheng, J. Zhou, and R. Qin, *Nano Lett* **12**, 113 (2012).
- [4] A. Arshad, M. Jabbal, Y. Yan, and D. Reay, (*Journal of Molecular Liquids*, 2019).
- [5] N. Kurra, Q. Jiang, P. Nayak, and H. N. Alshareef, *Nano Today* **24**, 81 (2019).
- [6] L. P. Lingamdinne, J. R. Koduru, and R. R. Karri, *Journal of environmental management* **231**, 622 (2019).
- [7] J. Liu, Q. Ma, Z. Huang, G. Liu, and H. Zhang, *Advanced Materials* **31**, 1800696 (2019).
- [8] V. B. Mohan, L. D. Hui, , and D. Bhattacharyya, *Composites Part B: Engineering* **142**, 200 (2018).
- [9] B. Qiu, M. Xing, and J. Zhang, *Chemical Society Reviews* **47**, 2165 (2018).
- [10] N. N. Rosli, M. A. Ibrahim, N. A. Ludin, M. A. M. Teridi, and K. Sopian, *Renewable and Sustainable Energy Reviews* **99**, 83 (2019).
- [11] R. N. Shah, A. E. Jakus, M. C. Hersam, and E. B. Secor, (Google Patents, ed, 2019).
- [12] C. H. A. Tsang, H. Huang, J. Xuan, H. Wang, and D. Leung, *Renewable and Sustainable Energy Reviews* **120**, 109656 (2020).
- [13] Z. Yang, J. Tian, Z. Yin, C. Cui, W. Qian, and F. Wei, *Carbon* **141**, 467 (2019).
- [14] Y. Zhang, X. Xia, B. Liu, S. Deng, D. Xie, and e. a. Q. Liu, *Advanced Energy Materials* , 1803342 (2019).
- [15] D. G. Papageorgiou, I. A. Kinloch, and R. J. Young, *Progress in Materials Science* **90**, 75 (2017).
- [16] N. A. A. Ghany, S. A. Elsherif, and H. T. Handal, *Surfaces and Interfaces* **9**, 93 (2017).
- [17] Y. Zhao, Li, X. Zhou, and Y.-n **231**, 324 (2016).
- [18] T. Mahmoudi, Y. Wang, and Y.-B. Hahn, *Nano Energy* **47**, 51 (2018).
- [19] B. Cai, C. Shao, L. Qu, Y. Meng, and L. Jin, *Frontiers of Materials Science* **13**, 145 (2019).
- [20] M. T. Hasan, R. Gonzalez-Rodriguez, C. Ryan, K. Pota, K. Green, and J. L. Coffer, *Nano Research* **12**, 1041 (2019).
- [21] Y. Luan, B. Yang, K. Zhu, S. Shao, Y. Gao, and K. Cheng, *ChemPlusChem* **10** (2019).
- [22] M. Tripathi, A. Markevich, R. B"ottger, S. Facsko, E. Besley, and J. Kotakoski, *ACS Nano* **12**, 4641 (2018).
- [23] P. Vogt, P. D. Padova, C. Quaresima, J. Avila, E. Frantzeskakis, and e. a. M. C. Asensio, *Physical review letters* **108**, 155501 (2012).
- [24] B. Lalmi, H. Oughaddou, H. Enriquez, A. Kara, S. Vizzini, and e. a. B. Ealet, *Applied Physics Letters* **97**, 223109 (2010).
- [25] L. Drissi, E. Saidi, M. Bousmina, and O. Fassi-Fehri, *Journal of Physics: Condensed Matter* **24** (2012).
- [26] H. Wu, Y. Qian, Z. Du, R. Zhu, E. Kan, and K. Deng, *Physics Letters A* **381**, 3754 (2017).
- [27] X. Chang, Q. Xue, D. He, L. Zhu, X. Li, and B. Tao, *International Journal of Hydrogen Energy* **42**, 24189 (2017).
- [28] D. Coello-Fiallos, T. Tene, J. L. Guayllas, D. Haro, A. Haro, and C. V. Gomez, *Materials Today: Proceedings* **4**, 6835 (2017).
- [29] E. D. Cantero, L. M. Solis, Y. Tong, J. D. Fuhr, M. L. Martiarena, and e. a. O. Grizzi, *Phys Chem Chem Phys* **19**, 18580 (2017).
- [30] W. Ju, T. Li, X. Su, H. Cui, and H. Li, *Applied Surface Science* **384**, 65 (2016).
- [31] L. Meng, Y. Wang, L. Zhang, S. Du, R. Wu, and e. a. L. Li, *Nano Lett* **13**, 685 (2013).
- [32] N. D. Drummond, V. Zólyomi, and V. I. Fal'ko, *Physical Review B* **85** (2012).
- [33] S. Li, Y. Wu, Y. Tu, Y. Wang, T. Jiang, and e. a. W. Liu, *Sci Rep* **5**, 7881 (2015).
- [34] M. J. Momeni, M. Mousavi-Khoshdeld, and E. Targholi, *Materials Chemistry and Physics* **192**, 125 (2017).
- [35] R. Das, S. Chowdhury, A. Majumdar, and D. Jana, *RSC Advances* **5**, 41 (2015).
- [36] S. Lin, S. Zhang, X. Li, W. Xu, X. Pi, and e. a. X. Liu, *The Journal of Physical Chemistry C* **119**, 19772 (2015).
- [37] H. Dong, B. Lin, K. Gilmore, T. Hou, S.-T. Lee, and Y. Li, *Journal of Power Sources* **299**, 371 (2015).
- [38] L. J. Zhou, Y. F. Zhang, and L. M. Wu, *Nano Lett* **13**, 5431 (2013).
- [39] H. Dong, L. Wang, L. Zhou, T. Hou, and Y. Li, *Carbon* **113**, 114 (2017).
- [40] M. Houmad, I. Essaoudi, A. Ainane, A. E. Kenz, A. Benyoussef, and R. Ahuja, *Optik* **177**, 118 (2019).
- [41] S. R. Naqvi, T. Hussain, W. Luo, and R. Ahuja, *Nano Research* **11**, 3802 (2018).
- [42] H. Dong, L. Zhou, T. Frauenheim, T. Hou, S.-T. Lee, and Y. Li, *Nanoscale* **8**, 6994 (2016).
- [43] Y. Ding and Y. Wang, *The Journal of Physical Chemistry C* **117**, 18266 (2013).
- [44] X. Tang, W. Liu, C. Luo, X. Peng, and J. Zhong, *RSC advances* **9**, 12276 (2019).
- [45] H. D. Pham, S.-Y. Lin, G. Gumbs, N. D. Khanh, and M.-F. Lin, *Frontiers in Physics* **8** (2020).
- [46] H.-D. Pham, S.-Y. Lin, G. Gumbs, N. D. Khanh, and M.-F. Lin, "Diversified properties of carbon substitutions in silicene," (2019), arXiv preprint, arXiv:1912.00334.
- [47] P. E. Bl"ochl, *Physical review B* **50**, 17953 (1994).
- [48] P. Giannozzi and J. P. Condens, *Matter* **21**, 1 (2009).
- [49] J. P. Perdew, K. Burke, and M. Ernzerhof, *Physical Review Letters* **77**, 3865 (1996).
- [50] H. J. Monkhorst and J. D. Pack, *Physical Review B* **13**, 5188 (1976).
- [51] H. Wang, M. Wu, X. Lei, Z. Tian, B. Xu, and e. a. K. Huang, *Nano Energy* (2018).
- [52] N. Gao, W. T. Zheng, and Q. Jiang, *Phys Chem Chem Phys* **14**, 257 (2012).
- [53] J. Zhao, H. Liu, Z. Yu, R. Quhe, S. Zhou, and e. a. Y. Wang, *Progress in Materials Science* **83**, 24 (2016).
- [54] L.-D. Zhang, F. Yang, and Y. Yao, *Scientific Reports* **5**, 8203 (2015).
- [55] S. Zhao, K. Yamamoto, S. Iikubo, S. Hayase, and T. Ma, *Journal of Physics and Chemistry of Solids* **117**, 117 (2018).
- [56] L. B. Drissi, F. Z. Ramadan, E. H. Saidi, M. Bousmina, and O. Fassi-Fehri, *Journal of the Physical Society of Japan* **82**, 104711 (2013).
- [57] J. S. Im, S.-J. Park, and Y.-S. Lee, *International Journal of Hydrogen Energy* **34**, 1423 (2009).
- [58] H. Zhang, M. Hu, Z.-H. Huang, F. Kang, and R. Lv, *Progress in Natural Science: Materials International* **30**, 13 (2020).
- [59] F. S. Gentile, A. Platonenko, K. E. El-Kelany, M. R  rat, P. D'Arco, and R. Dovesi, (*Journal of Computational Chemistry*, 2020).

- [60] Y. Mao, G. Guo, J. Yuan, and J. Zhong, *Applied Surface Science* **464**, 236 (2019).
- [61] Y. Wang and Y. Ding, *Solid State Communications* **155**, 6 (2013).
- [62] F. Wooten, Academic press: *Optical properties of solids* (2013).
- [63] P. Rani, G. S. Dubey, and V. K. Jindal, *Physica E: Low-dimensional Systems and Nanostructures* **62**, 28 (2014).
- [64] Q. Tan, P. Irwin, and Y. Cao, *IEEE Transactions on Fundamentals and Materials* **126**, 1153 (2006).
- [65] J. Chen, C. Li, and G. Shi, *The Journal of Physical Chemistry Letters* **4**, 1244 (2013).
- [66] S. R. C. Vivekchand, C. S. Rout, K. S. Subrahmanyam, A. Govindaraj, and C. N. R. Rao, *Journal of Chemical Sciences* **120**, 9 (2008).
- [67] M. Houmad, A. E. Kenz, and A. Benyoussef, *Optik* **157**, 936 (2018).
- [68] X. Chen, J. Jiang, Q. Liang, R. Meng, C. Tan, and Q. Yang, *Journal of Materials Chemistry C* **4**, 7004 (2016).
- [69] F. S. Rojas, C. B. Ojeda, and J. C. Pavon, *Talanta* **35**, 753 (1988).
- [70] J. de Wild, J. K. Rath, A. Meijerink, W. G. J. H. M. van Sark, and R. E. I. Schropp, "Enhanced near-infrared response of a-si:h solar cells with β -nayf4:yb3+ (18;".
- [71] H. Sun, Z. Guo, Y. Zhu, X. Li, L. Guan, and e. a. D. Peng, *Solar Energy Materials and Solar Cells* **205** (2020).
- [72] A. Baride, G. Sigdel, W. M. Cross, J. J. Kellar, and P. S. May, *ACS Applied Nano Materials* **2**, 4518 (2019).
- [73] S. Chen, J. Wu, A. Cai, N. Gonzalez, and R. Yin, *Neuroscience Research* **152**, 59 (2020).
- [74] Y. Hu, J. F. Honek, B. C. Wilson, and Q.-B. Lu, *Journal of Biophotonics* **12**, e201900129 (2019).
- [75] W. Qin, D. Zhang, D. Zhao, L. Wang, and K. Zheng, *Chemical Communications* **46**, 2304 (2010).
- [76] Y. Wang, Y.-Y. Huang, Y. Wang, P. Lyu, and M. R. Hamblin, *Scientific Reports* **7**, 7781 (2017).
- [77] W. T. Holcombe and M. Svajda, (Google Patents, ed, 2011).